H. J. Chu
Research Group of Mechanics,
Yanzhou University,
Yangzhou 225009, China;
Department of Civil Engineering,
University of Akron,
Akron, OH 44325

E. Pan[1]
Department of Civil Engineering,
University of Akron,
Akron, OH 44325
e-mail: pan2@uakron.edu

J. Wang
Materials Science and Technology Division,
Los Alamos National Laboratory,
Los Alamos, NM 87545

I. J. Beyerlein
Theoretical Division,
Fluid Dynamics and Solid Mechanics Division,
Los Alamos National Laboratory,
Los Alamos, NM 87545

Elastic Displacement and Stress Fields Induced by a Dislocation of Polygonal Shape in an Anisotropic Elastic Half-Space

The elastic displacement and stress fields due to a polygonal dislocation within an anisotropic homogeneous half-space are studied in this paper. Simple line integrals from 0 to π for the elastic fields are derived by applying the point-force Green's functions in the corresponding half-space. Notably, the geometry of the polygonal dislocation is included entirely in the integrand easing integration for any arbitrarily shaped dislocation. We apply the proposed method to a hexagonal shaped dislocation loop with Burgers vector along [$\bar{1}$ 1 0] lying on the crystallographic (1 1 1) slip plane within a half-space of a copper crystal. It is demonstrated numerically that the displacement jump condition on the dislocation loop surface and the traction-free condition on the surface of the half-space are both satisfied. On the free surface of the half-space, it is shown that the distributions of the hydrostatic stress $(\sigma_{11}+\sigma_{22})/2$ and pseudohydrostatic displacement $(u_1+u_2)/2$ are both anti-symmetric, while the biaxial stress $(\sigma_{11}-\sigma_{22})/2$ and pseudobiaxial displacement $(u_1-u_2)/2$ are both symmetric. [DOI: 10.1115/1.4005554]

Keywords: polygonal dislocation, displacement and stress fields, Green's function, anisotropic half-space

1 Introduction

Misfit dislocations often emerge during the fabrication of metal crystals [1,2], ceramic [3] and some high-performance nanostructures, such as quantum dots [4] and quantum wells [5]. Generation of such dislocations is an energetically favorable way for the material to relieve the strain energy induced by an inherent lattice mismatch or thermal mismatch. An important element of the problem of stress fields produced by misfit dislocations is the presence of a free surface [6]. For this reason, straight dislocations including edge and screw dislocations near a free surface have been well investigated for isotropic solids [7–11] and even anisotropic solids [12,13]. Assuming a three-dimensional (3D) isotropic half-space, Bacon and Groves [14] presented a surface integral for the stresses induced by an arbitrary dislocation, and Gosling and Willis [6] a line integral expression (along the dislocation boundary) for the stresses due to an arbitrary shaped dislocation. Special cases such as an angular dislocations [15] and dislocations inside an anisotropic elliptical inclusion [16] were also studied. Some other theory/method including the stress coupled theory [17] and multiscale method [18] were recently utilized to study the response of dislocations.

The elastic fields due to dislocation loops in a 3D anisotropic half-space can be expressed by the integrals of the point-force Green's function and its derivatives over the dislocation surfaces [6,18–20]. The point-force Green's function for an anisotropic half-space is often separated into two parts: the full-space part and the image part [6,21,22]. The surface integral of the full-space Green's function for the stress field can be reduced to a line integral using Stokes' theorem [23], or even to an analytical expression in the case of straight dislocation line segments [24,25]. However, an explicit expression for the second part, that is, the stresses relating to the image part of Green's function in the half-space, does not currently exist. In the study of the displacements due to dislocations, only the general surface integral over a dislocation loop has been derived where the point-force Green's function lies in its integrand [6,19]. Thus, a corresponding line integral expression for the image portion of the problem of a dislocation in an anisotropic 3D half-space is lacking. Reducing the surface integral to a line integral is crucial for efficient and accurate prediction of the dislocation-induced elastic fields. The major difficulty in reducing the surface integral to a line integral for the image displacement and stress fields due to dislocations in anisotropic materials is that Stokes' theorem cannot be utilized.

In this paper, we use the point-force Green's function in the Stroh formalism to derive line integrals (from 0 to π) for the elastic displacements and strains due to polygonal dislocations in an anisotropic 3D half-space. In these analytical line integrals, the influence of dislocation geometry on the displacement and strain fields is completely included in the integrands. This paper is organized as follows. In Sec. 2, some basic expressions for the displacements and stresses due to the dislocation loops and the point-force Green's function are reviewed. In section 3, line integral expressions for the elastic field including displacements and strains are derived by integrating the generalized triple integrals over a triangular dislocation, the fundamental dislocation element from which any polygonal dislocation can be constructed. In Sec. 4, the proposed integral expressions are then applied to calculate the elastic displacement and stress fields due to a hexagonal dislocation in a half-space of a single crystal with a face centered cubic (fcc) crystal structure. Lastly, we end with some discussion and conclusions.

2 Problem Description and Some Basic Formula

The problem is to predict the elastic field (displacements and stresses) due to a dislocation of polygonal shape with Burgers

[1]Corresponding author.

Contributed by the Applied Mechanics Division of ASME for publication in the JOURNAL OF APPLIED MECHANICS. Manuscript received December 2, 2010; final manuscript received April 25, 2011; accepted manuscript posted January 30, 2012; published online February 13, 2012. Assoc. Editor: Pradeep Sharma.

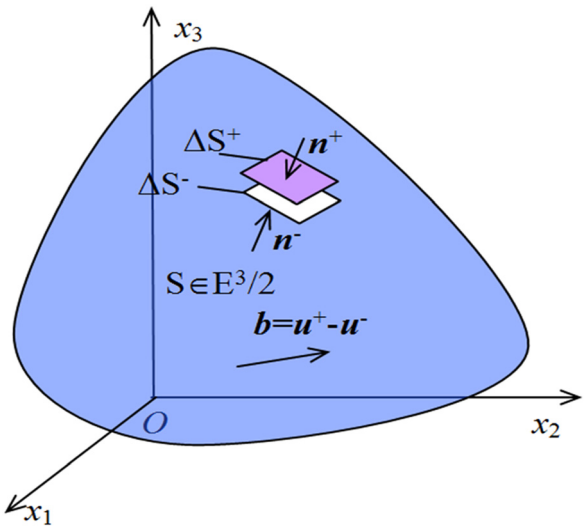

Fig. 1 Geometry of an arbitrarily shaped dislocation loop S in an anisotropic, elastic, and half-space $E^3/2$. The vector b denotes the Burgers vector of the dislocation, which is equal to the displacement jump across the dislocation surface. The vector n^+ denotes the normal of the surface S^+ towards S^-, and $n^- = -n^+$.

vector $\boldsymbol{b}$ within a 3D anisotropic elastic homogeneous half-space ($x_3 \geq 0$). The dislocation surface denoted by S is shown in Fig. 1 in the global coordinate system (O: x_1, x_2, x_3). The displacement discontinuity on S is described by dividing it into two adjacent surfaces: surface S^+ with unit normal $\boldsymbol{n}^+$ and S^- with unit normal $\boldsymbol{n}^-$. With this, the boundary/continuity condition in the infinity of the half-space, on the surface of the half-space ($x_3 = 0$), and across the dislocation surface S, can be specified, respectively, as follows:

$$\begin{cases} u_i|_{|x|\to\infty} = 0, \quad \sigma_{ij}\cdot n_j\big|_{x_3=0} = 0 \\ [u_i] \equiv u_i^+ - u_i^- = b_i \quad \text{and} \quad \sigma_{ij}^+\cdot n_j^+ + \sigma_{ij}^-\cdot n_j^- = 0 \text{ across } S \end{cases} \tag{1}$$

We adopt the Hooke's law for the constitutive relationship for an anisotropic material:

$$\sigma_{ij} = C_{ijkl}\varepsilon_{kl} \tag{2}$$

Throughout this paper, repeated indices obey the summation convention from 1 to 3, unless stated otherwise.

To solve the dislocation problem in terms of point-force Green's functions, we first consider two independent systems in the same anisotropic material, where one system is under a concentrated unit point force at $\boldsymbol{y}$, and the other one is the present dislocation problem described by Eq. (1). For the first, the governing equation is

$$\sigma_{ij,i}^k(\boldsymbol{y};\boldsymbol{x}) + \delta_{jk}\delta(\boldsymbol{x}-\boldsymbol{y}) = 0 \tag{3}$$

where $\sigma_{ij}^k(\boldsymbol{y};\boldsymbol{x})$ denotes the ij-component of the stress at $\boldsymbol{x}$ induced by a unit point force applied at $\boldsymbol{y}$ in the k-direction. For the second, the equilibrium equation is

$$\sigma_{ij,i}(\boldsymbol{x}) = 0 \tag{4}$$

We now apply Betti's reciprocal theorem to the two systems and arrive at the following well-known integral representation for the displacement field induced by the dislocation

$$u_k(\boldsymbol{y}) = \int_{\partial\Omega} [\sigma_{ij}(\boldsymbol{x})G_{jk}(\boldsymbol{y};\boldsymbol{x}) - \sigma_{ij}^k(\boldsymbol{y};\boldsymbol{x})u_j(\boldsymbol{x})]n_i(\boldsymbol{x})\mathrm{d}S(\boldsymbol{x}) \tag{5}$$

where $G_{jk}(\boldsymbol{y};\boldsymbol{x})$ is the Green's displacement in the j-direction at $\boldsymbol{x}$ induced by a point force in the k-direction applied at $\boldsymbol{y}$, and $\partial\Omega$ denotes the boundary of the half-space ($x_3 = 0$) and the dislocation surface S. According to the boundary conditions in Eq. (1), the contribution of the first integrand on the right-hand side of Eq. (4) is exactly zero. Thus, Eq. (4) becomes,

$$u_k(\boldsymbol{y}) = -\int_{S^+ + S^-} \sigma_{ij}^k(\boldsymbol{y};\boldsymbol{x})u_j(\boldsymbol{x})n_i(\boldsymbol{x})\mathrm{d}S(\boldsymbol{x}) \tag{6}$$

Applying the displacement discontinuity condition in Eq. (1), we obtain

$$u_k(\boldsymbol{y}) = \int_S \sigma_{ij}^k(\boldsymbol{y};\boldsymbol{x})b_j n_i \mathrm{d}S(\boldsymbol{x}) \tag{7}$$

where $n_i \equiv n_i^-$. Making use of the constitutive equation in Eq. (2), we finally have

$$u_k(\boldsymbol{y}) = \int_S C_{ijml}G_{mk,x_l}(\boldsymbol{y};\boldsymbol{x})b_j n_i \mathrm{d}S(\boldsymbol{x}) \tag{8}$$

It should be pointed out that $G_{mk}(\boldsymbol{y};\boldsymbol{x})$ represents the half-space Green's displacement in the m-direction at $\boldsymbol{x}$ induced by a point force in the k-direction applied at $\boldsymbol{y}$. Eq. (8) plays the important role in connecting the response of the dislocation to that of the point force in the half-space. Therefore, once the solution to the point-force Green's function is obtained, the corresponding dislocation problem can be solved. In the following, we apply the Fourier transform method to solve the point-force Green's function and the corresponding dislocation problem. To simplify the notation, symbols for tensors and vectors will be used when necessary.

Consider a point force vector $\boldsymbol{f}$ applied at $(0, 0, d)$ in an anisotropic homogeneous half-space ($x_3 \geq 0$). We divide the half-space into two parts at $x_3 = d$ (i.e., one part covers $x_3 > d$ and the other $0 \leq x_3 < d$) and apply the two-dimensional Fourier transforms to the system. In the Fourier space, the boundary conditions in Eq. (1) become

$$\begin{cases} \tilde{u}_i|_{x_3\to\infty} = 0, \quad \tilde{u}_i|_{x_3=d^+} - \tilde{u}_i|_{x_3=d^-} = 0 \\ \tilde{\sigma}_{ij}\cdot n_j\big|_{x_3=0} = 0, \quad \tilde{\sigma}_{ij}\cdot n_j\big|_{x_3=d^+} + \tilde{\sigma}_{ij}\cdot n_j\big|_{x_3=d^+} + f_i = 0 \end{cases} \tag{9}$$

where the displacement in the Fourier space is

$$\tilde{u}_k(\xi_1,\xi_2,x_3) = \int_{-\infty}^{+\infty}\int_{-\infty}^{+\infty} u_k(x_1,x_2,x_3)\,\mathrm{e}^{\mathrm{i}(x_1\xi_1+x_2\xi_2)}\mathrm{d}x_1\mathrm{d}x_2 \tag{10}$$

The equilibrium equation in the Fourier domain in a source-free region is

$$C_{i\alpha k\beta}\xi_\alpha\xi_\beta\tilde{u}_k + \mathrm{i}(C_{i\alpha k3} + C_{i3k\alpha})\xi_\alpha\tilde{u}_{k,3} - C_{i3k3}\tilde{u}_{k,33} = 0 \tag{11}$$

The general solution of Eq. (11) can be expressed as

$$\tilde{\boldsymbol{u}}(\xi_1,\xi_2,x_3) = \boldsymbol{a}\exp(-\mathrm{i}p\eta x_3) \tag{12}$$

where p and $\boldsymbol{a}$ are the eigenvalue and eigenvector of the Stroh eigenrelation (Ting, [21]), i.e.,

$$\left[\mathbf{Q} + p\left(\mathbf{R} + \mathbf{R}^T\right) + p^2\mathbf{T}\right]\boldsymbol{a} = 0 \tag{13}$$

with

$$\begin{aligned} &Q_{ij} = C_{ikjs}n_k n_s, \quad R_{ij} = C_{ikjs}n_k m_s, \quad T_{ij} = C_{ikjs}m_k m_s \\ &\boldsymbol{n} = [\cos\theta, \sin\theta, 0]^T, \quad \boldsymbol{m} = [0,0,1]^T, \quad \boldsymbol{\xi} = \eta\boldsymbol{n} \end{aligned} \tag{14}$$

where the superscript 'T' indicates the matrix transpose. With the eigenvalues and the associated eigenvectors p_i and $\boldsymbol{a}_i$ ($i=1, 2, \ldots, 6$), we let

$$\begin{aligned} &\mathrm{Im}(p_i) > 0, \quad p_{i+3} = \bar{p}_i, \quad \bar{\boldsymbol{a}}_{i+3} = \bar{\boldsymbol{a}}_i, \quad (i = 1,2,3) \\ &\mathbf{A} \equiv [\boldsymbol{a}_1, \boldsymbol{a}_2, \boldsymbol{a}_3], \quad \mathbf{B} \equiv [\boldsymbol{b}_1, \boldsymbol{b}_2, \boldsymbol{b}_3] \text{ with } \boldsymbol{b}_i \equiv \left(\mathbf{R}^T + p_i \mathbf{T}\right)\boldsymbol{a}_i \end{aligned} \tag{15}$$

where the symbol 'Im' and the overbar denote, respectively, the imaginary part and the complex conjugate of a complex variable. In this case, no summation is taken over the repeated index i in Eq. (15).

Making use of the displacement and traction conditions in Eq. (9), the elastic displacement vector in the transformed domain is found to be

$$\tilde{\boldsymbol{u}}(\xi_1, \xi_2, x_3) = \begin{cases} -\mathrm{i}\eta^{-1}\left[\bar{\mathbf{A}}\mathbf{H}_1(\bar{p}_*)\bar{\mathbf{A}}^T\boldsymbol{f} + \bar{\mathbf{A}}\mathbf{H}_2\mathbf{A}^T\boldsymbol{f}\right], & x_3 > d \\ \mathrm{i}\eta^{-1}\left[\mathbf{A}\mathbf{H}_1(p_*)\mathbf{A}^T\boldsymbol{f} - \bar{\mathbf{A}}\mathbf{H}_2\mathbf{A}^T\boldsymbol{f}\right], & 0 \le x_3 < d \end{cases} \tag{16}$$

with

$$\begin{aligned} &\mathbf{H}_1(p_*) \equiv \left\langle \mathrm{e}^{-\mathrm{i}p_*\eta(x_3-d)} \right\rangle \\ &\mathbf{H}_2 \equiv \left\langle \mathrm{e}^{-\mathrm{i}\bar{p}_*\eta x_3} \right\rangle \bar{\mathbf{B}}^{-1}\mathbf{B} \left\langle \mathrm{e}^{\mathrm{i}\bar{p}_*\eta d} \right\rangle \end{aligned} \tag{17}$$

where the symbol $\langle\cdot\rangle$ denotes the diagonal matrix. The subscript "*" takes 1, 2 and 3, which corresponds, respectively, to the first, second and third diagonal element.

Taking the Fourier inverse transform of Eq. (16), we arrive at the Green's displacement vector in the physical domain as

$$\boldsymbol{u}(\boldsymbol{x}) = \begin{cases} \dfrac{-\mathrm{i}}{4\pi^2}\displaystyle\iint \eta^{-1}\left[\bar{\mathbf{A}}\mathbf{H}_1(\bar{p}_*)\bar{\mathbf{A}}^T\boldsymbol{f} + \bar{\mathbf{A}}\mathbf{H}_2\mathbf{A}^T\boldsymbol{f}\right]\mathrm{e}^{-\mathrm{i}(x_1\xi_1 + x_2\xi_2)}\mathrm{d}\xi_1\mathrm{d}\xi_2, & x_3 > d \\ \dfrac{\mathrm{i}}{4\pi^2}\displaystyle\iint \eta^{-1}\left[\mathbf{A}\mathbf{H}_1(p_*)\mathbf{A}^T\boldsymbol{f} - \bar{\mathbf{A}}\mathbf{H}_2\mathbf{A}^T\boldsymbol{f}\right]\mathrm{e}^{-\mathrm{i}(x_1\xi_1 + x_2\xi_2)}\mathrm{d}\xi_1\mathrm{d}\xi_2, & 0 \le x_3 < d \end{cases} \tag{18}$$

To best manipulate the double integrals, the polar coordinate system is introduced. As seen below, this transformation allows integration over the radial variable to be carried out exactly. From Eq. (14), we have

$$\xi_1 = \eta\cos\theta; \quad \xi_2 = \eta\sin\theta \tag{19}$$

which converts Eq. (18) to

$$\boldsymbol{u}(\boldsymbol{x}) = \begin{cases} \dfrac{-\mathrm{i}}{2\pi^2}\displaystyle\int_0^{\pi}\mathrm{d}\theta\int_0^{\infty}\left[\bar{\mathbf{A}}\mathbf{H}_1(\bar{p}_*)\bar{\mathbf{A}}^T\boldsymbol{f} + \bar{\mathbf{A}}\mathbf{H}_2\mathbf{A}^T\boldsymbol{f}\right]\mathrm{e}^{-\mathrm{i}\eta(x_1\cos\theta + x_2\sin\theta)}\mathrm{d}\eta, & x_3 > d \\ \dfrac{\mathrm{i}}{2\pi^2}\displaystyle\int_0^{\pi}\mathrm{d}\theta\int_0^{\infty}\left[\mathbf{A}\mathbf{H}_1(p_*)\mathbf{A}^T\boldsymbol{f} - \bar{\mathbf{A}}\mathbf{H}_2\mathbf{A}^T\boldsymbol{f}\right]\mathrm{e}^{-\mathrm{i}\eta(x_1\cos\theta + x_2\sin\theta)}\mathrm{d}\eta, & 0 \le x_3 < d \end{cases} \tag{20}$$

Since $\boldsymbol{A}$ and $\boldsymbol{B}$ are independent of η, the integral over η can be carried out exactly. With this, the displacement vector can be finally expressed as

$$\boldsymbol{u}(\boldsymbol{x}) = \begin{cases} \dfrac{-1}{2\pi^2}\displaystyle\int_0^{\pi}\left[\bar{\mathbf{A}}\mathbf{Q}_1(\bar{p}_*)\bar{\mathbf{A}}^T + \bar{\mathbf{A}}\mathbf{Q}_2\mathbf{A}^T\right]\boldsymbol{f}\,\mathrm{d}\theta, & x_3 > d \\ \dfrac{1}{2\pi^2}\displaystyle\int_0^{\pi}\left[\mathbf{A}\mathbf{Q}_1(p_*)\mathbf{A}^T - \bar{\mathbf{A}}\mathbf{Q}_2\mathbf{A}^T\right]\boldsymbol{f}\,\mathrm{d}\theta, & 0 \le x_3 < d \end{cases} \tag{21}$$

where

$$\begin{aligned} [\mathbf{Q}_1(p_*)]_{ij} &= \frac{\delta_{ij}}{p_i(x_3 - d) + x_1\cos\theta + x_2\sin\theta} \\ (\mathbf{Q}_2)_{ij} &= \frac{\left(\bar{\mathbf{B}}^{-1}\mathbf{B}\right)_{ij}}{\bar{p}_i x_3 - p_j d + x_1\cos\theta + x_2\sin\theta} \end{aligned} \tag{22}$$

If the point-force vector $\boldsymbol{f}$ is applied at a general point $\boldsymbol{y}$, the expression for the displacement vector in Eq. (21) remains the same, while Eq. (22) should be modified to

$$\begin{aligned} [\mathbf{Q}_1(p_*)]_{ij} &= \frac{\delta_{ij}}{p_i(x_3 - y_3) + (x_1 - y_1)\cos\theta + (x_2 - y_2)\sin\theta} \\ (\mathbf{Q}_2)_{ij} &= \frac{\left(\bar{\mathbf{B}}^{-1}\mathbf{B}\right)_{ij}}{\bar{p}_i x_3 - p_j y_3 + (x_1 - y_1)\cos\theta + (x_2 - y_2)\sin\theta} \end{aligned} \tag{23}$$

As a result, the point-force Green's displacement tensor is given by

$$\boldsymbol{G}(\boldsymbol{y}, \boldsymbol{x}) = \begin{cases} \dfrac{-1}{2\pi^2}\displaystyle\int_0^{\pi}\left[\bar{\mathbf{A}}\mathbf{Q}_1\bar{\mathbf{A}}^T + \bar{\mathbf{A}}\mathbf{Q}_2\mathbf{A}^T\right]\mathrm{d}\theta, & x_3 > y_3 \\ \dfrac{1}{2\pi^2}\displaystyle\int_0^{\pi}\left[\mathbf{A}\mathbf{Q}_1\mathbf{A}^T - \bar{\mathbf{A}}\mathbf{Q}_2\mathbf{A}^T\right]\mathrm{d}\theta, & 0 \le x_3 < y_3 \end{cases} \tag{24}$$

It is observed that the Green's function solution for the displacement contains two parts. The first part corresponds to the Green's function in the full space, while the second part is the image one, which is induced by the free surface of the half-space. Notably, the full-space part of the Green's function depends only on material properties. In what follows, we will use this expression to derive the elastic fields due to a dislocation of polygonal shape in a general homogeneous, elastically anisotropic 3D half-space.

3 The Elastic Fields Induced by a Dislocation of Polygonal Shape

A triangular shape serves as the fundamental unit for any polygon. An arbitrary polygonal surface can always be approximated by a summation of triangular elements. Therefore, the solution of a dislocation of polygonal shape can then be obtained from the solution of a dislocation of triangular shape via the method of

superposition. With this in mind, we first derive the solution induced by a dislocation of triangular shape. Because of the importance of this solution, we will denote the associated quantities by a superscript triangle symbol.

Consider the triangular dislocation shown in Fig. 2. Let the maximum value of x_3 on the dislocation loop be $x_{3\max}$ and the minimum x_3 be $x_{3\min}$. Substituting Eq. (24) into Eq. (8) gives the following expression for the displacement induced by a triangular dislocation

$$u_k^{\Delta_i}(\boldsymbol{y}) = \begin{cases} \dfrac{-1}{2\pi^2}\displaystyle\int_0^{\pi} \mathrm{d}\theta \int_{\Delta_i} C_{ijml}\left[\bar{\mathbf{A}}\mathbf{Q}_1(\bar{p}_*)\bar{\mathbf{A}}^T + \bar{\mathbf{A}}\mathbf{Q}_2\mathbf{A}^T\right]_{mk,l} b_j n_i \mathrm{d}S(\boldsymbol{x}) & y_3 > x_{3\max} \\ \dfrac{1}{2\pi^2}\displaystyle\int_0^{\pi} \mathrm{d}\theta \int_{\Delta_i} C_{ijml}\left[\mathbf{A}\mathbf{Q}_1(p_*)\mathbf{A}^T - \bar{\mathbf{A}}\mathbf{Q}_2\mathbf{A}^T\right]_{mk,l} b_j n_i \mathrm{d}S(\boldsymbol{x}) & y_3 < x_{3\min} \end{cases} \tag{25}$$

Since the eigenvector matrix $\boldsymbol{A}$ is independent of the variable on the surface of the triangle, the area integration over the triangle in Eq. (25) can be carried out first for the solution of the displacement

$$u_k^{\Delta_i}(\boldsymbol{y}) = \begin{cases} \dfrac{-1}{2\pi^2}\displaystyle\int_0^{\pi} \left[C_{ijml} b_j n_i \bar{A}_{mt}\left(\bar{A}_{sk}^T D_{1tsl}^{\Delta_i}(\bar{p}_*) + A_{sk}^T D_{2tsl}^{\Delta_i}\right)\right]\mathrm{d}\theta, & y_3 > x_{3\max} \\ \dfrac{1}{2\pi^2}\displaystyle\int_0^{\pi} \left[C_{ijml} b_j n_i A_{sk}^T\left(A_{mt} D_{1tsl}^{\Delta_i}(p_*) - \bar{A}_{mt} D_{2tsl}^{\Delta_i}\right)\right]\mathrm{d}\theta, & y_3 < x_{3\min} \end{cases} \tag{26}$$

where

$$\begin{aligned} D_{1tsl}^{\Delta_i}(\bar{p}_*) &\equiv \int_{\Delta_i} Q_{1ts,x_l}(\bar{p}_*)\mathrm{d}S(\boldsymbol{x}) = \int_{\Delta_i} \frac{-\delta_{ts} h_l(\bar{p}_t)}{[\boldsymbol{h}(\bar{p}_t)\cdot(\boldsymbol{x}-\boldsymbol{y})]^2}\mathrm{d}S(\boldsymbol{x}) \\ D_{2tsl}^{\Delta_i} &\equiv \int_{\Delta_i} Q_{2ts,x_l}\mathrm{d}S(\boldsymbol{x}) = \int_{\Delta_i} \frac{-\left(\bar{\mathbf{B}}^{-1}\mathbf{B}\right)_{ts} h_l(\bar{p}_t)}{[\boldsymbol{h}(\bar{p}_t)\cdot\boldsymbol{x} - \boldsymbol{h}(p_s)\cdot\boldsymbol{y}]^2}\mathrm{d}S(\boldsymbol{x}) \end{aligned} \tag{27}$$

and where the vector $\boldsymbol{h}$ is defined as

$$\boldsymbol{h}(p) = [\cos\theta, \sin\theta, p]^T \tag{28}$$

The corresponding strain is simply the derivative of the displacement solution, Eq. (26), i.e.,

$$u_{k,p}^{\Delta_i}(\boldsymbol{y}) = \begin{cases} \dfrac{-1}{2\pi^2}\displaystyle\int_0^{\pi} \left[C_{ijml} b_j n_i \bar{A}_{mt}\left(\bar{A}_{sk}^T J_{1tslp}^{\Delta_i}(\bar{p}_*) + A_{sk}^T J_{2tslp}^{\Delta_i}\right)\right]\mathrm{d}\theta, & y_3 > x_{3\max} \\ \dfrac{1}{2\pi^2}\displaystyle\int_0^{\pi} \left[C_{ijml} b_j n_i A_{sk}^T\left(A_{mt} J_{1tslp}^{\Delta_i}(p_*) - \bar{A}_{mt} J_{2tslp}^{\Delta_i}\right)\right]\mathrm{d}\theta, & y_3 < x_{3\min} \end{cases} \tag{29}$$

where

$$\begin{aligned} J_{1tslp}^{\Delta_i}(\bar{p}_*) &\equiv D_{1tsl,y_p}^{\Delta_i}(\bar{p}_*) = \int_{\Delta_i} \frac{-2\delta_{ts} h_l(\bar{p}_t) h_p(\bar{p}_t)}{[\boldsymbol{h}(\bar{p}_t)\cdot(\boldsymbol{x}-\boldsymbol{y})]^3}\mathrm{d}S(\boldsymbol{x}) \\ J_{2tslp}^{\Delta_i} &\equiv D_{2tsl,y_p}^{\Delta_i} = \int_{\Delta_i} \frac{-2\left(\bar{\mathbf{B}}^{-1}\mathbf{B}\right)_{ts} h_l(\bar{p}_t) h_p(p_s)}{[\boldsymbol{h}(\bar{p}_t)\cdot\boldsymbol{x} - \boldsymbol{h}(p_s)\cdot\boldsymbol{y}]^3}\mathrm{d}S(\boldsymbol{x}) \end{aligned} \tag{30}$$

Comparing Eq. (27) to Eq. (30), we observe that the denominators in the integrands of J_2 and D_2 can be, respectively, degenerated to those in J_1 and D_1 by letting $p_s = \bar{p}_t$. Thus, we only need to analyze integrals J_2 and D_2. Moreover, since the numerators of the integrands in the expressions of J_2 and D_2 are independent of $\boldsymbol{x}$, their integrals are simply the power functions of -2 and -3. The power order is determined by the derivative order applied to the Green's displacement function. For the $(n-1)$-order derivative, the power order is n. Accordingly, the kernel integral on the triangular dislocation is generally

$$F_n^{\Delta_i}(p*, q*) = \int_{\Delta_i} \frac{\mathrm{d}S(\boldsymbol{x})}{[\boldsymbol{h}(p*)\cdot\boldsymbol{x} - \boldsymbol{h}(q*)\cdot\boldsymbol{y}]^n} \tag{31}$$

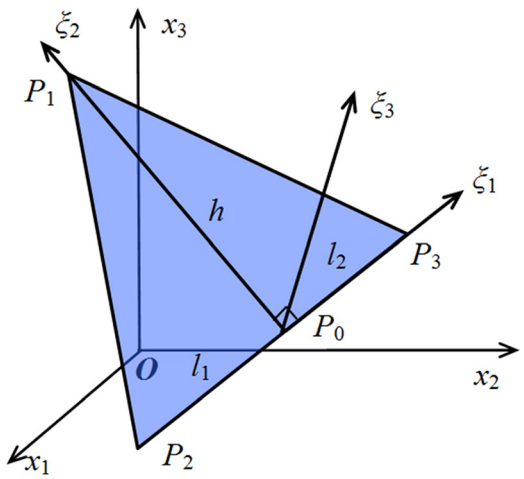

Fig. 2 Geometry of a triangular dislocation with corners P_1, P_2, P_3 with respect to the global coordinate system (O; x_1,x_2,x_3) and local coordinate system (x_0; ξ_1, ξ_2, ξ_3) where $h = \xi_2(P_1)$, $l_1 = -\xi_1(P_2)$, $l_2 = \xi_1(P_3)$. Lengths l_1 and l_2 can also be negative.

where p^* and q^* can be assigned to different eigenvalues. It is important to note that in Eqs. (26), (29) and (31), the influence of the triangular shape of the dislocation on the displacements and strains induced by the dislocation is mainly contained in the integral, Eq. (31). Therefore the function $F_n^{\Delta_i}$ can be appropriately named the n-th order shape factor. When $n=2$, $F_n^{\Delta_i}$ is the shape factor for the displacement, and when $n=3$, it is the shape factor for the corresponding strain.

In order to carry out the area integration in Eq. (31), the local coordinate system ($\boldsymbol{P_0}$: ξ_1,ξ_2,ξ_3) with the base vectors $\boldsymbol{\xi}_i^0$ ($i=1,2,3$) shown in Fig. 2 is introduced. The base vectors in the corresponding global coordinate system ($\boldsymbol{O}$: x_1,x_2,x_3) are $\boldsymbol{x}_i^0$ ($i=1,2,3$). The transformation matrix between the local and global systems is therefore

$$D_{ij} = \boldsymbol{x}_i^0 \cdot \boldsymbol{\xi}_j^0 \tag{32}$$

The integral in Eq. (31) is then rewritten as

$$F_n^{\Delta_i}(p*,q*) = \int_0^h d\xi_2 \int_{-l_1+l_1\xi_2/h}^{l_2-l_2\xi_2/h} \times \frac{d\xi_1}{[\mathrm{f}_1(p*,q*)\xi_1 + \mathrm{f}_2(p*,q*)\xi_2 + \mathrm{f}_3(p*,q*)]^n} \tag{33}$$

where

$$f_\alpha(p*,q*) = D_{k\alpha}h_k(p*), \quad \alpha = 1,2 \tag{34}$$

$$f_3(p*,q*) = h_k(p*)P_{0k} - h_k(q*)y_k \tag{35}$$

Integration of Eq. (33) for n = 2 and 3 gives

$$F_2^{\Delta_i}(p*,q*) = \frac{1}{f_1}\left(\frac{1}{f_2+f_1l_1^*}\ln\frac{f_3^*+f_2}{f_3^*-f_1l_1^*} - \frac{1}{f_2-f_1l_2^*}\ln\frac{f_3^*+f_2}{f_3^*+f_1l_2^*}\right)$$

$$F_3^{\Delta_i}(p*,q*) = \frac{1}{2}\frac{l_1^*+l_2^*}{h(f_3^*+f_2)(f_3^*+f_1l_2^*)(f_3^*-f_1l_1^*)} \tag{36}$$

with

$$l_1^* = l_1/h, \quad l_2^* = l_2/h, \quad f_3^* = f_3/h \tag{37}$$

For a polygonal dislocation constructed by N distinct (nonoverlapping) triangles, the shape factors are

$$F_n(p*,q*) = \sum_{n=1}^{N} F_n^{\Delta_i}(p*,q*) \tag{38}$$

Using Eqs. (26), (29) and (38), we finally obtain the following displacement field due to the polygonal dislocation,

$$u_k(\boldsymbol{y}) = \begin{cases} \dfrac{-1}{2\pi^2}\displaystyle\int_0^\pi \left[C_{ijml}b_jn_i\bar{A}_{mt}\left(\bar{A}_{sk}^T D_{1tsl}(\bar{p}_*) + A_{sk}^T D_{2tsl}\right)\right]\mathrm{d}\theta, & y_3 > x_{3\max} \\ \dfrac{1}{2\pi^2}\displaystyle\int_0^\pi \left[C_{ijml}b_jn_iA_{sk}^T\left(A_{mt}D_{1tsl}(p_*) - \bar{A}_{mt}D_{2tsl}\right)\right]\mathrm{d}\theta, & y_3 < x_{3\min} \end{cases} \tag{39}$$

where

$$D_{1tsl}(\bar{p}_*) = -\delta_{ts}h_l(\bar{p}_t)F_2(\bar{p}_t,\bar{p}_t)$$
$$D_{2tsl} = -\left(\bar{\mathbf{B}}^{-1}\mathbf{B}\right)_{ts}h_l(\bar{p}_t)F_2(\bar{p}_t,p_s) \tag{40}$$

The corresponding strain field is

$$u_{k,p}(\boldsymbol{y}) = \begin{cases} \dfrac{-1}{2\pi^2}\displaystyle\int_0^\pi \left[C_{ijml}b_jn_i\bar{A}_{mt}\left(\bar{A}_{sk}^T J_{1tslp}(\bar{p}_*) + A_{sk}^T J_{2tslp}\right)\right]\mathrm{d}\theta, & y_3 > x_{3\max} \\ \dfrac{1}{2\pi^2}\displaystyle\int_0^\pi \left[C_{ijml}b_jn_iA_{sk}^T\left(A_{mt}J_{1tslp}(p_*) - \bar{A}_{mt}J_{2tslp}\right)\right]\mathrm{d}\theta, & y_3 < x_{3\min} \end{cases} \tag{41}$$

where

$$J_{1tslp}(\bar{p}_*) = -2\delta_{ts}h_l(\bar{p}_t)h_p(\bar{p}_t)F_3(\bar{p}_t,\bar{p}_t)$$
$$J_{2tslp} = -2\left(\bar{\mathbf{B}}^{-1}\mathbf{B}\right)_{ts}h_l(\bar{p}_t)h_p(p_s)F_3(\bar{p}_t,p_s) \tag{42}$$

The solutions presented here have two outstanding features. First, the generalized triple integrals for dislocation-induced displacements and strains have been reduced to a more mathematically convenient form of line integrals. Second, in either integral, Eq. (39) or integral, Eq. (41), the solution includes both the contribution from the full-space and from the image part, similar to the one given in Eq. (24).

We must also emphasize that Eqs. (25) and (29) and those derived based on them are not suitable for $y_3 \in (x_{3\min}, x_{3\max})$. To deal with this issue, we consider separately the contribution from the full-space and image parts in the integrals for the strains when $y_3 \in (x_{3\min}, x_{3\max})$. Let us consider the contribution of the image part first. Based on the Green's function in Eq. (24), it can easily be seen that the image part is continuous, signifying that the contribution of the image part in the integral for the strain is the same as that in Eq. (41). The contribution of the full-space part in the strain, however, is dealt with in a different way. The strategy in this case is to transform the integral of the full-space part to a new coordinate system and carry out the integral under this system. In this new coordinate system, the x_3-axis is designated as the normal of the dislocation surface. This gives $x_{3\max} = x_{3\min}$ on the dislocation, allowing the contribution of full-space part at any point in the full space to be evaluated by following the same procedure as that in Eq. (41). Accordingly, the derived formula will have the same form as the contribution of the full-space part in Eq. (41). In this treatment all material and geometrical properties, such as

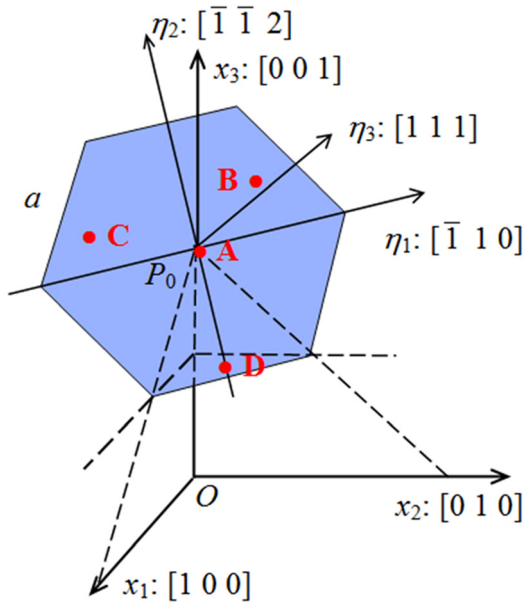

Fig. 3 Geometry of a regular hexagon dislocation where (O; x_1,x_2,x_3) is the global coordinate system and (P_0; η_1, η_2, η_3) the local dislocation coordinate system

C_{ijml}, b_j, n_i and the positions of the vertex of the polygons must also be transformed to the new coordinate system. After obtaining the contribution of the full-space part under the new coordinates, then it is desirable to transform them back to the original global coordinates. This general approach also can be used to evaluate the dislocation-induced displacement field.

4 Numerical Examples

In this section, the displacements and stress fields induced by a hexagonal shaped dislocation lying within a half-space of a copper single crystal are analyzed by the new line-integral expressions derived in the present work. In face-centered cubic (fcc) crystals like copper, dislocation glide occurs along the {1 1 1} slip planes in the $\langle\bar{1}\ 1\ 0\rangle$ slip direction. Without loss of generality, the hexagonal dislocation with the side length a in the present problem is placed on the (1 1 1) slip plane and its Burgers vector $\boldsymbol{b}$ is parallel to [$\bar{1}$ 1 0] within this plane (Fig. 3). The distance between the center of the hexagonal dislocation and the free surface of the half-space is $4a$. Figure 3 shows the relationship between the local dislocation coordinates (η_i; $i=1,2,3$) and the global coordinates (x_i; $i=1,2,3$) as well as the locations of the four points A, B, C, D in our numerical calculation. For convenience, the displacements and stresses are normalized according to

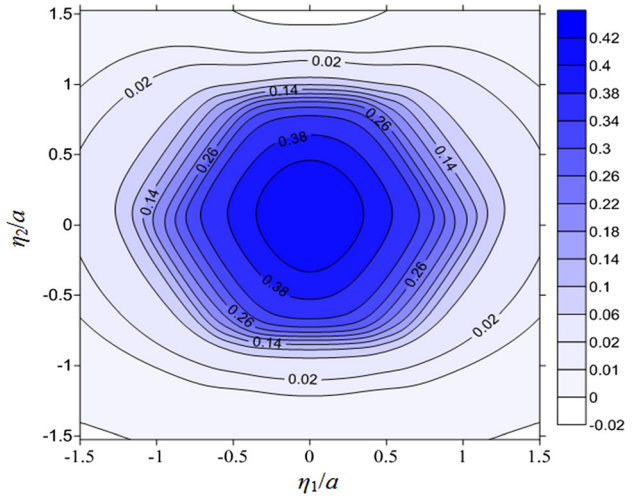

Fig. 4 Contour map of the normalized local displacement component u_1/b in local coordinates η_1/a and η_2/a induced by a regular hexagonal dislocation, where b is the magnitude of the Burgers vector

$$\tilde{u}_i = u_i/b$$
$$\tilde{\sigma}_{ij} = \frac{a}{b}\frac{\sigma_{ij}}{C_{\max}} \equiv \frac{\sigma_{ij}}{\lambda C_{\max}} \tag{43}$$

where $C_{\max} = C_{11}$ is used to normalize the stress and b is the magnitude of the Burgers vector $\boldsymbol{b}$. The local and global coordinates are normalized to

$$\tilde{\eta}_i = \eta_i/a$$
$$\tilde{x}_i = x_i/a \tag{44}$$

Numerical results for this problem are provided in Table 1 and Figs. 4–12, and are discussed next.

4.1 Validation on Boundary Conditions. The correctness of the proposed solution is first evaluated by checking the displacement discontinuity condition across the dislocation surface S and the traction-free boundary condition on the free surface of the half-space. For the former, the displacement jump between the upper S^+ and lower S^- surfaces of the dislocation should equal the Burgers vector $\boldsymbol{b}$. The displacements at the four different points $A=(0,\ 0,\ 0)$, $B=(0.5,\ 0.4,\ 0)$, $C=(-0.6,\ 0.3,\ 0)$ and $D=(0,-0.7,\ 0)$ on the dislocation surface are calculated in the local η_i ($i=1,\ 2,\ 3$) coordinates (Fig. 3). Specifically, the adjacent points on opposing sides of the dislocation surface associated with each one are $A^{\pm}=(0,\ 0,\ \pm\eta_3)$, $B^{\pm}=(0.5,\ 0.4,\ \pm\eta_3)$, $C^{\pm}=(-0.6,\ 0.3,\ \pm\eta_3)$ and $D^{\pm}=(0,-0.7,\ \pm\eta_3)$, where these coordinates have

Table 1 Numerical results of the displacement jump at points A, B, C, and D on the dislocation plane. All data are given in local coordinates (η_i; $i=1,2,3$) and normalized by the Burgers vector. The superscript "+" and subscript "–" denote, respectively, the points in the upper and lower surfaces of the dislocation.

Points	u_1	u_2	u_3	Δu_1	Δu_2	Δu_3
A^+	0.49522099	-0.13893237×10^{-6}	0.95624814×10^{-7}	0.99835285	$<10^{-10}$	$<10^{-10}$
A^-	−0.50313186	-0.13893237×10^{-6}	0.95624814×10^{-7}			
B^+	0.49782604	-0.24133535×10^{-2}	0.43768557×10^{-1}	1.00318332	$<10^{-8}$	$<10^{-9}$
B^-	−0.50535728	-0.24133536×10^{-2}	0.43768557×10^{-1}			
C^+	0.49497190	-0.22339585×10^{-3}	-0.54283613×10^{-1}	0.99763493	$<10^{-10}$	$<10^{-9}$
C^-	−0.50266303	-0.22339588×10^{-3}	-0.54283613×10^{-1}			
D^+	0.49390064	-0.16506397×10^{-3}	0.38993962×10^{-3}	0.99458002	$<10^{-9}$	$<10^{-10}$
D^-	−0.50067938	-0.16506446×10^{-3}	0.38993969×10^{-3}			

Note: $A^{\pm}=(0,\ 0,\ \pm\eta_3)$, $B^{\pm}=(0.5,0.4,\ \pm\eta_3)$, $C^{\pm}=(-0.6,\ 0.3,\ \pm\eta_3)$, $D^{\pm}=(0,\ 0-.7,\ \pm\eta_3)$ where $\eta_3=10^{-7}$.

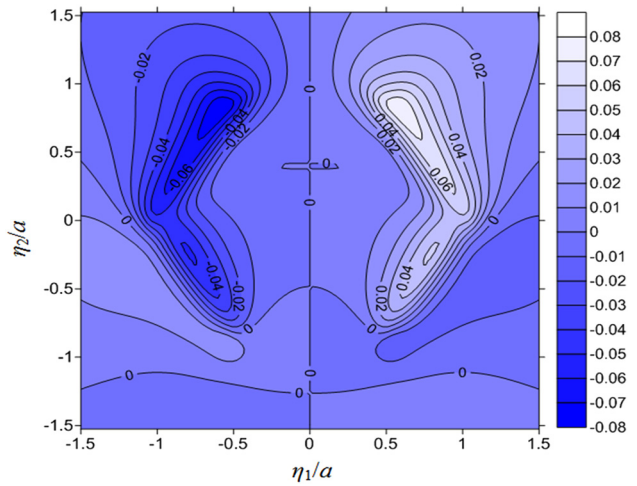

Fig. 5 Contour map of the normalized local displacement component u_2/b in local coordinates η_1/a and η_2/a induced by a regular hexagonal dislocation, where b is the magnitude of the Burgers vector

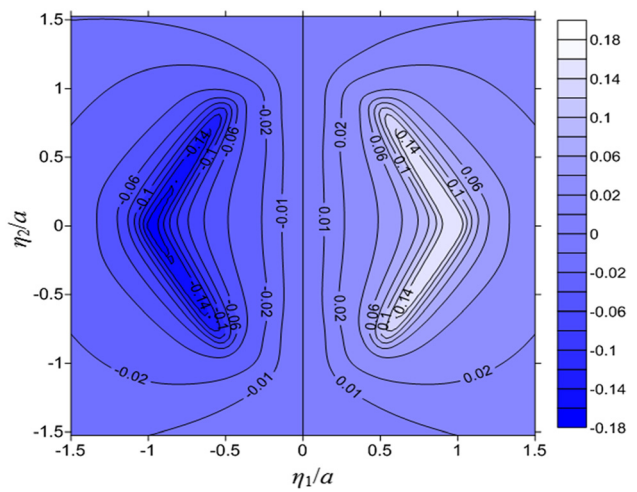

Fig. 6 Contour map of the normalized local displacement component u_3/b in local coordinates η_1/a and η_2/a induced by a regular hexagonal dislocation, where b is the magnitude of the Burgers vector

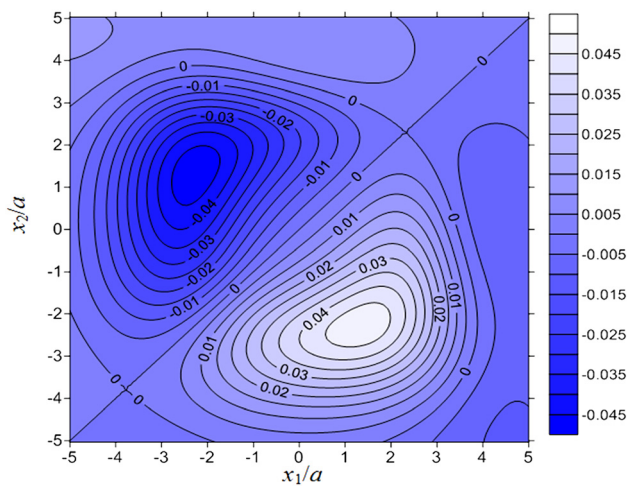

Fig. 7 Contour map of $(\sigma_{11}+\sigma_{22})/2$ normalized according to Eq. (43) in global coordinates, where the coordinates are normalized by the side length a of the hexagonal dislocation with Burgers vector of magnitude b

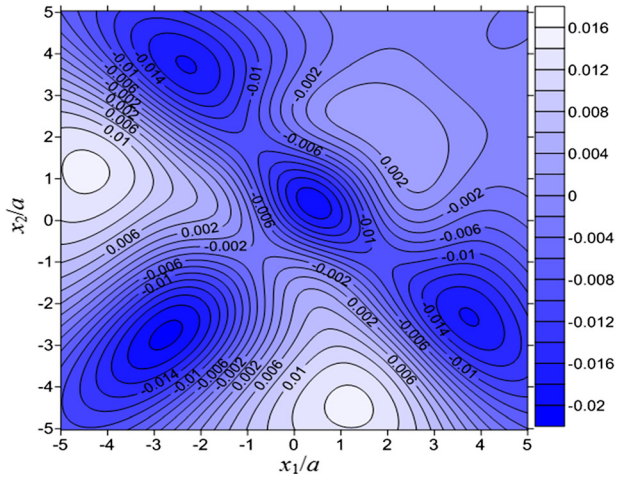

Fig. 8 Contour map of $(\sigma_{11}-\sigma_{22})/2$ normalized according to Eq. (43) in global coordinates, where the coordinates are normalized by the side length a of the hexagonal dislocation with Burgers vector of magnitude b

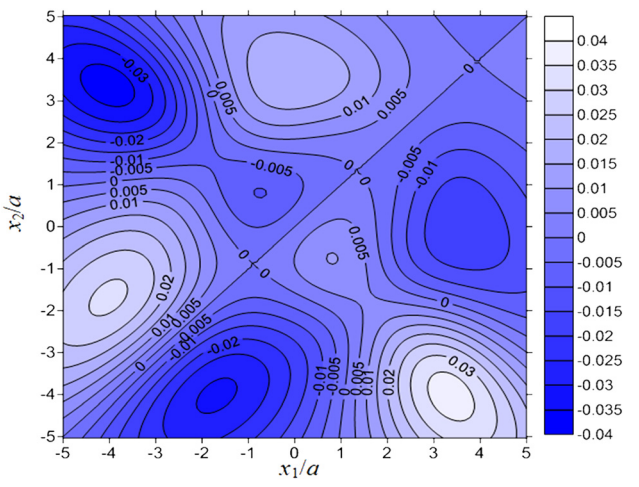

Fig. 9 Contour map of the normalized stress component σ_{12} (normalized according to Eq. (43)) in global coordinates, normalized by the side length a of the hexagonal dislocation with Burgers vector of magnitude b

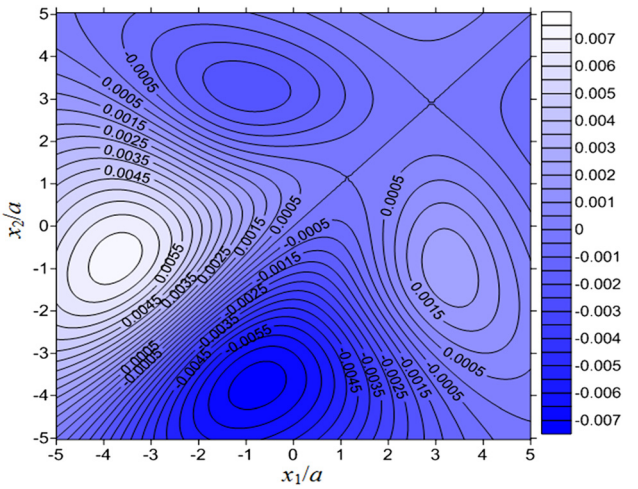

Fig. 10 Contour map of the normalized displacement $(u_1 + u_2)/2b$ in the normalized global coordinates x_1/a and x_2/a induced by a regular hexagonal dislocation with Burgers vector of magnitude b

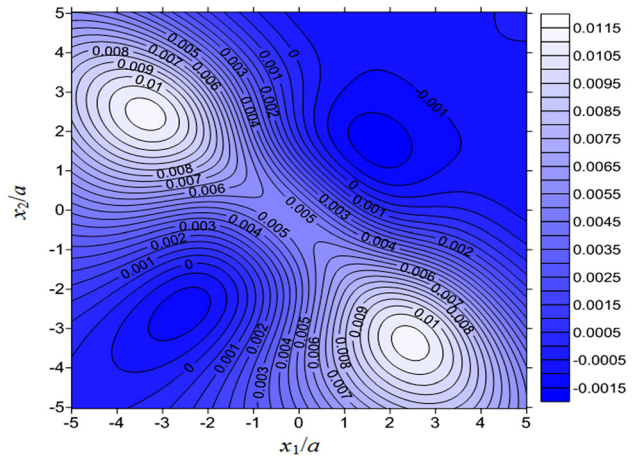

Fig. 11 Contour map of the normalized displacement $(u_1-u_2)/2b$ in the normalized global coordinates x_1/a and x_2/a induced by a regular hexagonal dislocation with Burgers vector of magnitude b

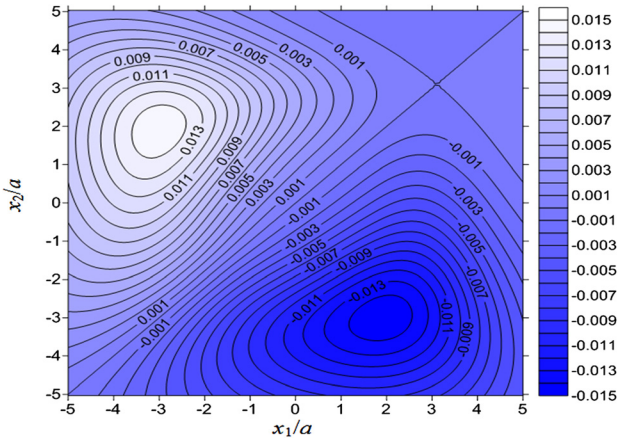

Fig. 12 Contour map of the normalized displacement u_3/b in the normalized global coordinates x_1/a and x_2/a induced by a regular hexagonal dislocation with Burgers vector of magnitude b

been normalized by a and $\eta_3 = 10^{-7}$. The numerical results are listed in Table 1, and are compared to the given Burgers vector along the local η_1-direction. They clearly show that the displacement jump at these four points nearly coincide with the Burgers vector with a relative error in the displacement along η_1 being below 0.5%. We mention that more accurate results can be obtained by increasing the Gaussian points for the line integral from 0 to π, and/or by further subdividing the triangles into more regular ones. The displacements along the η_2- and η_3-directions are extremely small (below 10^{-8}), which is to be expected since there is no slip along the η_2- and η_3-directions.

We have also randomly selected some points on the surface of the half-space in order to calculate the stress. It is shown that the magnitudes of the normalized tractions on the surface of the half-space are all below 10^{-8}. Therefore, the traction-free condition is also satisfied.

4.2 Displacement Field on the Dislocation Plane. For demonstration, displacements and stresses on the local plane $\eta_3 = 0.1a$ are calculated. Figures 4–6 show the distributions of the normalized displacements u_1, u_2 and u_3, respectively, in the local coordinate system. As shown in Fig. 4, the distribution of the displacement u_1 is symmetric about the local axis η_2, while the distribution of displacements u_2 and u_3 in Figs. 5–6 are anti-symmetric. It should be noted that the symmetric or anti-symmetric characteristics of the induced fields strongly depend on the Burgers vector. In our examples, the Burgers vector is assumed to be along the $[\bar{1}\ 1\ 0]$ direction. If, for instance, the Burgers vector is assumed to be along the local η_2-axis, i.e., the $[\bar{1}\ \bar{1}\ 2]$ direction, then the displacement u_2 will be symmetric about η_2, while the displacement u_1 becomes anti-symmetric. It should be also noted that the magnitude of the displacement u_1 at the center of the dislocation is nearly two orders of magnitude larger than others, except for near the corners of the hexagon.

4.3 Displacement and Stress Fields on the Free Surface. As mentioned in Sec. 4.1, our calculations using the present method verify that σ_{13}, σ_{23} and σ_{33} on the free surface of the half-space are close to zero. The distributions of the remaining stress components on the free surface of the half-space in global coordinates are presented in Figs. 7–9. While both the σ_{11} and σ_{22} distributions are asymmetrical, the distributions of the hydrostatic stress $\sigma_h = (\sigma_{11}+\sigma_{22})/2$ (Fig. 7) and biaxial stress $\sigma_b = (\sigma_{11}-\sigma_{22})/2$ (Fig. 8) possesses obvious symmetry characteristics about the global line $x_2 = x_1$. The former is anti-symmetric and the latter is symmetric. The distribution of σ_{12} (Fig. 9) in global coordinates is also anti-symmetric about $x_2 = x_1$.

Similar to the stresses, the distributions of the individual displacement components u_1 and u_2 in the global coordinates do not exhibit any particular symmetry property. However, the distribution of $u_h = (u_1+u_2)/2$, called the pseudohydrostatic displacement, and the distribution of $u_b = (u_1-u_2)/2$, the pseudobiaxial displacement, possess anti-symmetric and symmetric properties, respectively, as shown in Figs. 10–11. The u_3 distribution on the free surface shown in Fig. 12 is anti-symmetric about the line $x_2 = x_1$ and reaches its peak value around the points $(x_1, x_2) = (2, -3)$ and $(-3, 2)$ on the free surface $(x_3 = 0)$.

5 Discussions and Conclusions

In this paper, explicit expressions of the elastic displacement and stress fields due to an arbitrary dislocation loop in an anisotropic homogenous half-space are derived in terms of simple line integrals (from 0 to π). In the proposed integrals the influence of the shape of the polygonal dislocation on the elastic displacement and stress fields are all analytically contained in the integrand. Reduction from a surface integral to a line integral greatly improves the efficiency and accuracy on the calculation of the dislocation-induced elastic fields.

Based on the proposed method, the displacement and stress fields due to a hexagonal dislocation in a half-space of a copper crystal are obtained. Both the validity and precision of the method are well demonstrated by comparing the calculated displacement jump at the dislocation surface to the given Burgers vector and by checking the traction-free boundary condition on the free surface of the half-space. Results are also presented for the displacements and stresses on the global free surface of the half-space. These results could serve as benchmarks for numerical studies (utilizing, for instance, the finite element method) of similar dislocation problems in anisotropic crystals. The observed symmetric and anti-symmetric features of the elastic field distributions can provide insight when analyzing the influence and behavior of misfit dislocations present near free surfaces.

We mention that while the proposed unified integral interval (0, π) is more convenient to carry out and is furthermore independent of the loop shape, special numerical schemes are needed for handling the situation where the dislocation loop intersects with the free surface of the half space [26,27]. For example, the self-energy of an elliptic dislocation loop was derived in anisotropic elastic media and further corrected for one-dimensional core/shell nanowires by combining the boundary element method [26]. This solution was successfully in predicting the critical shell thickness corresponding to the defect-free core/shell nanowires [26].

Acknowledgment

This work was supported by the National Natural Science Foundation (10602050) and Jiangsu Government Scholarship for overseas studies. J. Wang and I. J. Beyerlein acknowledge support provided by Los Alamos National Laboratory Directed Research and Development (LDRD) Project No. DR20110029. J. Wang also acknowledges support provided by the U.S. Department of Energy, Office of Science, Office of Basic Energy Sciences and a Los Alamos National Laboratory Directed Research and Development (LDRD) Project No. ER20110573. The authors further sincerely thank Professor John Hirth for his comments on the dislocation singularity issue.

References

[1] Elbaum, C., 2009, "Dislocations in Metal Crystals Grown from the Melt," J. Appl. Phys. **31**, pp. 1413–1415.
[2] Li, X., Wei, Y., Lu, L., Lu, K., and Gao, H., 2010, "Dislocation Nucleation Governed Softening and Maximum Strength in Nano-Twinned Metals," Nature **464**, pp. 877–880.
[3] Ghosha, D., Subhasha, G., and Bourneb, G. R., 2009, "Room-Temperature Dislocation Activity During Mechanical Deformation of Polycrystalline Ultra-High-Temperature Ceramics," Scr. Mater. **61**, pp. 1075–1078.
[4] Ovid'ko, I. A., and Sheinerman, A. G., 2004, "Misfit Dislocation Loops in Cylindrical Quantum Dots," J. Phys.: Condens. Matter **16**, pp. 7225–7232.
[5] Passow, T., Maier, M., Kunzer, M., Leancu, C., Liu, S., Wiegert, J., Schmidt, R., Köhler, K., and Wagner, J., 2009, "Influence of Substrate Dislocation Density and Quantum Well Width on the Quantum Efficiency of Violet-Emitting GaInN/GaN Light-emitting Diodes," Phys. Status Solidi C **6**, pp. S833–S836.
[6] Gosling, T. J., and Willis, J. R., 1994, "A Line-Integral Representation for the Stresses due to an Arbitrary Dislocation in an Isotropic Half-Space," J. Mech. Phys. Solids **42**, pp. 1199–1221.
[7] Head, A. K., 1953, "Edge Dislocations in Inhomogeneous Media," Proc. Phys. Soc. London, Sect. B **66**, pp. 793–801.
[8] Willis, J. R., Jain, S. C., and Bullough, R., 1990, "The Energy of an Array of Dislocations: Implications for Strain Relaxation in Semiconductor Heterostructures," Philos. Mag. A **62**, pp. 115–129.
[9] Hirth, J. P., and Lothe, J., 1982, *Theory of Dislocations*, 2nd ed., Wiley, New York.
[10] Gutkin, M. Y., and Romanov, A. E., 1992, "Misfit Dislocations in a Thin Two-Phase Hetero-Epitaxial Plate," Phys. Status Solidi A **129**, pp. 117–126.
[11] Wang, X., and Sudak, L. J., 2006, "Interaction of a Screw Dislocation with an Arbitrary Shaped Elastic Inhomogeneity," J. Appl. Mech. **73**, pp. 206–211.
[12] Gosling, T. J., and Willis, J. R., 1993, "The Energy of Arrays of Dislocations in an Anisotropic Half-Space," Philos. Mag. A **69**, pp. 65–90.
[13] Ting, T. C., and Barnett, D. M., 1993, "Image Force on Line Dislocations in Anisotropic Elastic Half-Spaces with a Fixed Boundary," Int. J. Solids Struct. **30**, pp. 313–323.
[14] Bacon, D. J., and Crocker, A. G., 1965, "The Elastic Energies of Symmetrical Dislocation Loops," Philos. Mag. **12**, pp. 195–198.
[15] Comninou, M., and Dundurs, J., 1975, "The Angular Dislocation in a Half Space," J. Elasticity **5**, pp. 203–216.
[16] Yen, W. J., Hwu, C., and Liang, Y. K., 1995, "Dislocation Inside, Outside, or on the Interface of an Anisotropic Elliptical Inclusion," J. Appl. Mech. **62**, pp. 306–311.
[17] Shankar, M. R., Chandrasekar, S., and Farris, T. N., 2004, "Interaction Between Dislocations in a Couple Stress Medium," J. Appl. Mech. **71**, pp. 546–550.
[18] Elkhodary, K., Sun, L., Irving, D. L., Brenner, D. W., Ravichandran, G., and Zikry, M. A., 2009, "Integrated Experimental, Atomistic, and Microstructurally Based Finite Element Investigation of the Dynamic Compressive Behavior of 2139 Aluminum," J. Appl. Mech. **76**, p. 051306.
[19] Volterra, V., 1907, "Sur L'équilibre des Corps élastiques Miltiplement Connexes," Annales Scientifiques de l'École Normale Supérieure **24**, pp. 401–517.
[20] Han, X., and Ghoniem, N. M., 2005, "Stress Field and Interaction Forces of Dislocations in Anisotropic Multilayer Thin Films," Philos. Mag **85**, pp. 1205–1225.
[21] Ting, T. C. T., *Anisotropic Elasticity: Theory and Applications* (Oxford University, New York, 1996).
[22] Pan, E., and Yuan, F. G., 2000, "Three-Dimensional Green's Functions in Anisotropic Bimaterials," Int. J. Solids Struct. **37**, pp. 5329–5351.
[23] Mura, T., 1987, *Micromechanics and Defects in Solids*, 2nd ed., Kluwer, Boston.
[24] Willis, J. R., 1970, "Stress Fields Produced by Dislocations in Anisotropic Media," Philos. Mag. **21**, pp. 931–949.
[25] Wang, C. Y., 1996, "The Stress Field of a Dislocation Loop in an Anisotropic Solid," J. Mech. Phys. Solids. **44**, pp. 293–305.
[26] Chu, H. J., Wang, J., Zhou, C. Z., and Beyerlein, I. J., 2011, "Self-energy of Elliptical Dislocation Loops in Anisotropic Crystals and Its Application for Defect-free Core/Shell Nanowires," Acta Mater. **59**, pp. 7114–7124.
[27] Chu, H. J., Pan, E., Han, X., Wang, J., and Beyerlein, I. J., 2011, "Elastic Fields of Dislocation Loops in Three-Dimensional Anisotropic Bimaterials," J. Mech. Phys. Solids, available at http://www.sciencedirect.com/science/article/pii/S0022509611002407, last accessed 23 December 2011.